

Brain Dynamic Information Flow Estimation Based on EEG and Diffusion MRI

A Proof-of-principle Study and Application in Stroke

By

Runfeng Tian

in partial fulfilment of the requirements for the degree of

Master of Science

in Mechanical Engineering

at the Delft University of Technology,

to be defended publicly on Thursday August 30, 2018 at 2:30 PM.

Supervisor: Prof. dr. Frans C.T. van der Helm
Dr. ir. Yuan Yang

Thesis committee: Prof. dr. Frans C.T. van der Helm, TU Delft
Dr. ir. Yuan Yang, Northwestern University
MSc. Olena G. Filatova, TU Delft
Dr. ir. Daan M. Pool, TU Delft

This thesis is confidential and cannot be made public until August 30, 2020.

An electronic version of this thesis is available at <http://repository.tudelft.nl/>.

Contents

Abstract	3
1 Introduction.....	4
2 Data acquisition.....	8
2.1 Subjects.....	8
2.2 Electrical finger stimulation and EEG acquisition	9
2.3 MRI acquisition and preprocessing.....	11
3 Data analysis.....	12
3.1 EEG preprocessing.....	13
3.2 The forward problem.....	14
3.2.1 Co-register EEG and MRI coordinates.....	15
3.3 The inverse problem	16
3.4 Fiber tracking.....	19
3.5 Dynamic information flow estimation	20
3.6 Model evaluation.....	22
4 Results.....	24
5 Discussion.....	31
6 Conclusion.....	34
Bibliography	35

Abstract

In the hemiparetic stroke, functional recovery of paretic limb may occur with the reorganization of neural networks in the brain. Electroencephalography (EEG), with an excellent temporal resolution, can be used to reveal functional changes in the brain following a stroke. This study assessed a novel multimodal brain imaging technique namely Variational Bayesian Multimodal Encephalography (VBMEG), which combines EEG, anatomical MRI and diffusion weighted imaging (DWI), to estimation brain dynamic information flow and its changes following a stroke. EEG data were acquired from individuals suffering from a stroke as well as able-bodied participants while electrical stimuli were delivered sequentially at their index finger in the left and right hand, respectively. The locations of active sources related to this stimulus were precisely identified, resulting in high Variance Accounted For (VAF above 80%). An accurate estimation of dynamic information flow between sources was achieved in this study, showing a high VAF (above 88%) in the cross-validation test. The estimated dynamic information flow was compared between chronic hemiparetic stroke and able-bodied individuals, using matrices lateralization index and activation complexity. The results demonstrate the feasibility of VBMEG method in revealing the changes of information flow in the brain after stroke. This study verified the VBMEG method as an advanced computational approach to track the dynamic information flow in the brain following a stroke. This may lead to the development of a quantitative tool for monitoring functional changes of the cortical neural networks after a unilateral brain injury and therefore facilitate the research into, and the practice of stroke rehabilitation.

1 Introduction

Stroke is one of the top causes of disability-adjusted life years (DALY) lost. According to the information from World Health Organization in 2016, more than 1,5 million people suffer a stroke in Europe every year. In the Netherlands, demographic changes in the population suggest an increase of 27% in number of stroke patients per 1000 in 2020 compared with 2000 (Struijs et al., 2005). Meanwhile, the average age of ischemic stroke onset is decreasing with the increasing incidence among people below 50-year-old (Maaijwee et al., 2014), which means that the average DALY for each stroke survivor is increasing. Stroke survivors usually have problems with mobility, fatigue, speech, memory and/or emotions among others. These problems affect their ability to complete daily activities at home and to participate in the community. Among the disability patients caused by stroke, 25% to 30% are younger than 55 years (Smajlović, 2015), and less than 20% can go back to their normal professional and private life (Di Carlo, 2009). Thus, it is necessary to find rehabilitation methods for stroke patients.

The causes of stroke as well as the lesion size and position are different for each stroke patient. Stroke occurs when the blood supply to part of the brain is interrupted or severely reduced, the oxygen and nutrients for brain tissues are deprived, causing the brain cells start to die within minutes. There are two main types of stroke: ischemic and hemorrhagic stroke. Ischemic strokes are caused by interruption of the blood supply to the brain, while hemorrhagic strokes are due to bleeding within the skull. In the acute phase of stroke, over two-thirds of patients present with motor symptoms such as (hemi-)paresis or loss of dexterity (Kwakkel et al., 2002). Over 80% of the stroke survivors and more than 40% of the patients in the chronic stage suffer the hemiparesis of the contralateral limb (Ahn et al., 2015). Upper extremity motor deficiencies, including muscle weakness, changes in muscle tone, laxity etc., affect many daily life activities (Lang et al., 2013). The degree of upper extremity function is the main clinical predictor of whether a patient comes back to work or not. Clinical tests, such as Fugl-Meyer scores, indicate the severity of neural impairment following a stroke, but do not provide insight to the changes within the brain that occur after the incident and during recovery (Gladstone et al., 2002). Understanding how the brain reconfigures itself following a stroke is important for design effective and individualized rehabilitation method.

The recovery of brain function is realized by the neuroplasticity, which allows the neurons adjust their activities and build new connections according to the environment after injury (Arya et al., 2011, Murphy and Corbett, 2009). In the few months after acute stroke, recovery from motor deficits is predominantly driven by neuronal restitution and substitution (Grefkes and Fink, 2011, Rothi and Horner, 1983). Neuronal restitution assumes the increasing integrity of the injured functional system, while neuronal

substitution assumes the improvement results from system reorganization or compensation. During the recovery processes, brain connectivity is rebuilt or enhanced. Brain connectivity refers to anatomical, functional and effective connectivity. Anatomical connectivity describes the structure of anatomical links between brain areas. Functional connectivity is defined as temporal correlation (statistical dependence) between brain areas (Fingelkurts et al., 2005). While effective connectivity refers to the direct or indirect influence, also called causal interactions, of one brain area to another (Breakspear, 2004). Comparing with effective connectivity, functional connectivity cannot provide information about causal relationships between two or more areas. Brain effective connectivity can be achieved by tracking the information flow through the neural fibers within the brain network. One of the main strategies to investigate the brain effective connectivity is analyzing brain response to external stimuli. This can be achieved with various non-invasive brain imaging techniques such as electroencephalography (EEG) and functional magnetic resonance imaging (fMRI) (Bandara et al., 2016, Weinstein et al., 2018).

EEG measures the scalp voltage produced by electrical currents occurring naturally in the brain. The EEG signal originates from the net effect of ionic currents flowing in the dendrites of neurons during synaptic transmission. Mapping from the measured scalp EEG signals to their cortical sources is called an inverse problem, which is inherently ill-posed due to a limited number of measurement electrodes in comparison to the large number of active sources in the cortex (Wendel et al., 2009). Thus, precise source localization is a key challenge for EEG technique. Despite its poor spatial resolution, the major advantage of EEG is its temporal resolution in the order of milliseconds, which allows capturing the fast dynamics of brain activity.

Functional MRI measures the changes of blood flow in the brain based on the blood-oxygen-level dependent (BOLD) contrast. When the neuronal population is active, the blood flow increases and brings more oxygen. As a result, magnetic properties of the blood change in the corresponding brain areas. The spatial resolution of fMRI is in the order of 2-3 mm, which is much higher than that of EEG. However, the temporal resolution of fMRI is relatively low because the hemodynamic response reaches its peak around 5-6 seconds after the neural activity. Previous experiments shown that somatosensory evoked potential (SEP) spreads inside brain, starting from primary somatosensory cortex, within 200ms. EEG are more capable to investigate the SEP information flow than fMRI. Besides the consideration of temporal resolution, fMRI is very sensitive to head motion during measurement. The participants must hold still, which is probably hard for stroke patients. For these reasons, EEG is preferable in SEP experiments with stroke patients.

Other types of MR imaging mainly provide the anatomical brain information and have been proven to be clinically relevant, versatile tools. For example, T1-weighted anatomical acquisitions allow to obtain the high-resolution detailed brain structure. And diffusion-weighted MRI (dMRI) is typically used to infer white matter connections

between cortical regions. These image modalities have been successfully used to characterize the brain structure and the anatomic neural connections in both able-bodied individuals and people suffering from the stroke.

Each brain imaging technique has its pros and cons. Nowadays, it has been getting clear that combining different imaging modalities may improve our understanding of the brain as a complex biological system and its functions (Arikan, 2011). The underdetermined nature of the inverse problem of EEG calls for structural, physiological and functional information to be combined to better estimate the location of active sources in the brain and the causal interactions between sources, i.e. effective connectivity related to a specific form of stimulus. Various computational approaches such as dynamic causal modelling (DCM) and conditional Granger causality analysis have been proposed and used to estimate the effective connectivity (Bajaj et al., 2015, Schulz et al., 2016, Wang et al., 2016). However, most of the current methods either require the prior assumption on the model structure (e.g. DCM) or exclusively rely on the signal correlations without considering the anatomical constrain in the modelling (e.g. Granger causality analysis). Among the state-of-the-art methods, the Variational Bayesian Multimodal Encephalography (VBMEG) method has shown potential both in locating the active cortical sources and identifying the neural pathways (both physically and causally) connecting the active cortical sources. A physiologically constrained Bayesian estimation algorithm is used to locate active brain sources. Combining them with white matter tracks estimated from dMRI, a multivariate autoregressive (MAR) model is built to infer causal interactions between the active cortical sources (Friston, 2011a). Such a method allows tracking the information flow through the neural fibers within the brain network. The VBMEG method was initially proposed to investigate the dynamic cortical activity of healthy participants during a face recognition task (Fukushima et al., 2015). Nevertheless, as a novel brain imaging method, the clinical value of the VBMEG method is yet to be demonstrated, especially regarding its potential to investigate functional brain changes following a brain disease such as a stroke.

Therefore, the present work serves two aims: First, this is a proof of principle study validating the feasibility of the VBMEG method to estimate the active cortical sources and their dynamic interactions in stroke participants during a sensory stimulation task. The high-density EEG, structural MRI and diffusion MRI data were collected from both able-bodied and stroke participants. EEG was recorded when the participants were receiving an electrical finger stimulation. The accuracy of EEG source localization and dynamic information flow estimation within the VBMEG method was evaluated by the Variance Accounted For (VAF). The VAF indicates how much cortical activity and brain dynamics can be explained by the VBMEG method. The estimated dynamic information flow was compared between two chronic hemiparetic stroke survivors and two able-bodied individuals to demonstrate the feasibility of the VBMEG method in revealing functional cortical network changes post stroke. Second, application of the VBMEG method gives a visualization of brain dynamic information flow for both able-

bodied and stroke participants. This visualization intuitively shows the changes of how brain reacting with a stimulus post stroke. Besides, two metrics, lateralization index and activation complexity, were applied to examine the differences of brain information flow of able-bodied and stroke participants quantitatively. Lateralization index indicates hemispheric dominance for certain stimulus, and activation complexity implies percentage of active fibers among all fibers which connect ROIs.

The proof-of-principle study is a critical prerequisite for applying the VBMEG on a large database to identify a quantitative biomarker for assessing neurological impairment and exploring neurobiological recovery following a stroke. Also, the visualization of brain dynamic information flow has potential to help doctors and therapies without an engineering background make use of EEG and diffusion MRI. The designed metrics fill the gap that convention clinical tests cannot take insight into brain function and its changes after stroke, and they can be used to evaluate recovery and optimize treatments.

2 Data acquisition

2.1 Subjects

Two chronic stroke survivors and two age-matched able-bodied individuals were included in this study. The participants were recruited with informed consent and permission of the Medical Ethics Committee of the Vrije Universiteit Medical Center, Amsterdam. The trial protocol was registered on 23 October 2013 at the Netherlands Trial Register (identifier NTR4221). Inclusion criteria for the subjects suffering from chronic stroke were 1) upper limb paresis, 2) ability to sit without support (National Institutes of Health Stroke Scale item 5a/b > 0), 3) age over 18, 4) single ischemic hemispheric stroke, 5) more than six months post stroke. Exclusion criteria were 1) previously existing pathological neurological conditions or orthopedic limitations of the upper limb that would affect the results, 2) botulin toxin injections or medication that may have influenced upper limb function in the past three months, 3) general MRI contraindications (claustrophobia, pacemaker or other metallic implants), and 4) absence of history of epilepsy or seizures. All participants are in the age range of 55-70 in this study. The information of lesion side in the brain and clinical assessment for stroke survivors is provided in **Table 1**. Both stroke patients have lesions in the posterior limb of internal capsule, but in different hemispheres, as shown in **Figure 1**.

Subject	Lesion side	FM-UE	EmNSA	Year of stroke
Stroke 1	Right	58	8	2009
Stroke 2	Left	66	8	2009

Table 1 Information of stroke subjects. FM: Fugl-Meyer Upper Extremity Assessment Score, EmNSA: the Erasmus MC modification of the Nottingham Sensory Assessment

EEG and MRI measurements were not performed simultaneously, but on different dates. EEG was recorded in a measurement van which was designed so that the measurements could be done at locations convenient for the study participants. MR images were acquired after EEG at VUmc, Amsterdam, for both patients and healthy controls. The stroke participants were chronic patients with measurements done more than 6 years since stroke, meaning that clinically they reached their maximum recovery.

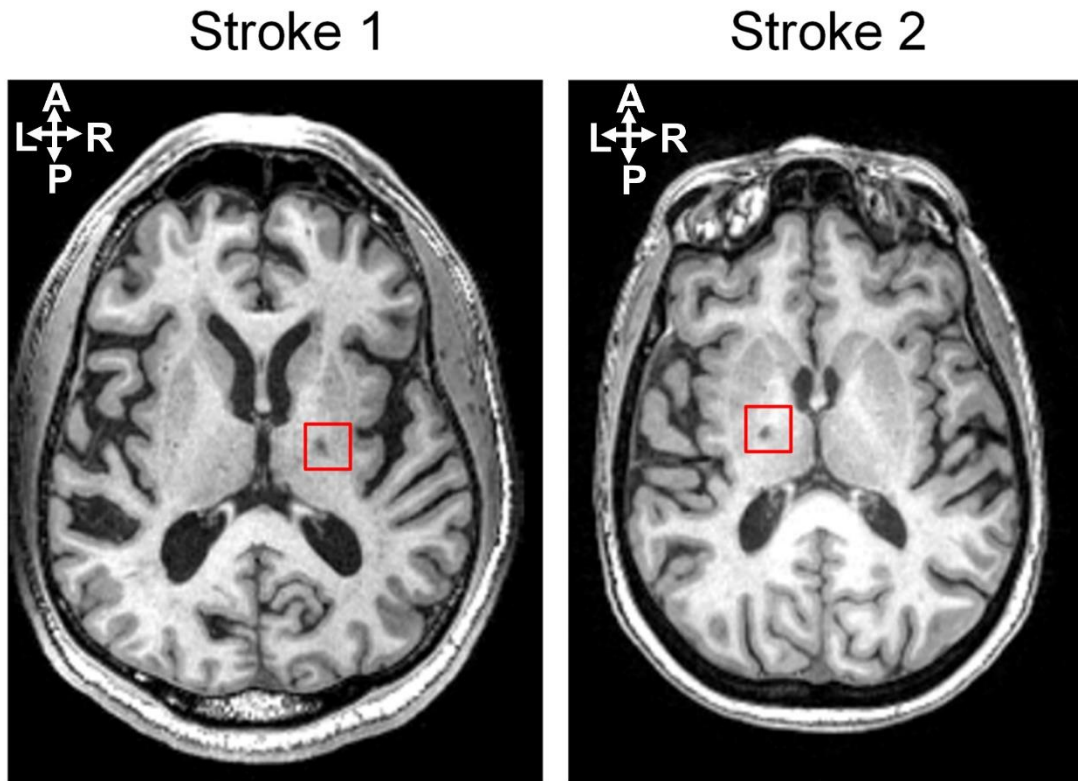


Figure 1 T1-MR imaging for two stroke participants. The lesions caused by stroke is marked out by red square. Both lesions are small, but right in the middle of the cortico-spinal tract.

2.2 Electrical finger stimulation and EEG acquisition

The experiment was performed within a NEN1010 approved measurement van. During the experiment, participants were sitting comfortably with their hands and forearms positioned on their lap with the fingers facing upward (supine position). Between forearm and lap, a pillow was placed to secure a stable position and comfort. Index fingers of both hands were stimulated with a randomized order in healthy controls and stroke patients with bipolar stimulation using a battery-powered electrical stimulator (Micromed, Brain quick, Treviso, Italy). The anodal electrode (size 1 cm) was placed on most distal phalange and cathode on the second distal phalange with an inter-electrode distance of approximately 1cm. This placement is chosen to reduce the likelihood of anodal block. Set up of the bipolar electrodes is shown in **Figure 2**. A monophasic anodic rectangular electrical pulse of 400 μ s width and a stimulation intensity of two times the sensation threshold was chosen. The sensation threshold was defined as the level at which the subject was able to sense half of the 10 given pulses. The stimulation was repeated 500 trials for each hand. The chosen stimulation did not cause any pain or heat feeling to the participants. During the stimulation, the EEG data were recorded with a 64-channel EEG system (TMSi, Netherlands) with ground electrode placed at the left mastoid, and online referenced to the common average. Sampling rate was 1024 Hz. Apart from antialiasing filters, no other filters

were applied online. Positions of the EEG electrodes for every subject were measured with the ANT Neuro Xensor system (ANT Neuro, Enschede, Netherlands).



Figure 2 Set up of the bipolar electrodes on the index finger of right hand

Electroencephalography (EEG) measures the electric fields produced by electrical currents occurring naturally in the brain. The EEG signal is primarily generated by the synaptic currents. The neuronal membranes act as tiny sources or sinks, where the current flows outward or inward respectively. For each neuron, the net current inflow and outflow through its membranes are zero based on the Kirchhoff's first law. When analyzing electric fields measured by noninvasive sensors (e.g. EEG electrodes), the neurons are assumed to be current sources and sinks separated spatially on the cortex. While the field generated from a single neuron is too weak to detect by EEG electrodes outside scalp, only neurons aligned within a volume of tissue with synaptic current flows correlated in time can be measured. The EEG signals represent the linear superposition of the fields generated by all such synaptic currents across all neurons. A demonstration of generation of electric fields and measurement of EEG electrodes is shown in **Figure 3**.

Among all the neurons inside human brain, cortical pyramidal cells generate electric fields which can be measured by EEG most easily, since cortical pyramidal cells are systematically aligned in a columnar fashion perpendicular to the cortical sheet. The current source or sink distribution within a small slab of cortex can thus be represented as a current dipole, which orients perpendicularly to the local cortical surface (Dale and Sereno, 1993). The orientation of the dipole is assumed to be perpendicular to the cortical sheet, and the dipole moment can be represented by a scalar function $S(r, t)$, reflecting dipole strength or moment as a function of location r and time t . The signal measured by EEG electrodes on scalp $\mathbf{M} = [m_1, m_2, \dots, m_N]$ and dipole moments $\mathbf{S} =$

$[s_1, s_2, \dots, s_p]$ ideally follows the relationship

$$\mathbf{M} = \mathbf{L}\mathbf{S}$$

where N and p indicate the number of EEG electrodes and dipoles respectively. \mathbf{L} is called leadfield matrix, which is derived from solving the forward problem based on the brain anatomical information and Kirchhoff's first law. Estimating dipole moments from EEG measurements and leadfield is called the inverse problem.

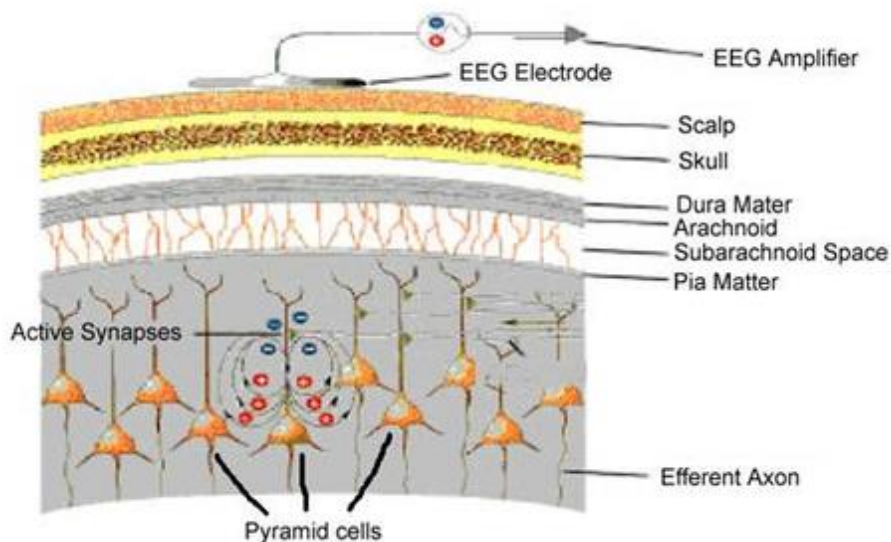


Figure 3 Generation of electrical fields by synaptic currents in pyramidal cells and measurement of EEG electrode outside scalp (Bear et al., 2007)

2.3 MRI acquisition and preprocessing

Image acquisition was performed with a 3T MRI scanner (Discovery MR750, GE Medical Systems) at VU University Medical Center. Anatomical T1-weighted acquisition had the following settings: TE=3.22 ms, TR=8.21 ms, flip angle 12°, imaging matrix = 256 x 256 x 172, resolution 1 mm³. The diffusion-weighted MRI (dMRI) acquisition protocol involved 40 non-collinear gradient directions uniformly sampled over a sphere for each of two b-values: 1000 and 2000 s/mm²; TE=100 ms, TR=7200 ms, pixel size 2.5x2.5 mm², 52 consecutive slices with a thickness of 2.5 mm, acquisition time 12,5 min. This allowed for whole brain coverage. Data for each b-value were acquired as separate scans together with five non-diffusion weighted images (i.e., per b-value).

3 Data analysis

This section explains the details of the VBMEG method, of which the workflow is shown in **Figure 4**. EEG, T1 and diffusion weighted MRIs are first preprocessed. Then a head model and a cortex model are built based on T1 MRI for each subject. Leadfield matrix is constructed with the head and cortex models as well as the EEG electrodes coordinates. The process of building leadfield matrix is called the forward problem. Then sources are estimated using hierarchical Variational Bayesian (hVB) approach with preprocessed EEG and leadfield matrix. This process is called the inverse problem. By combining sources and anatomical connection information from diffusion MRI, the Multivariate Autoregressive model is built leading to the estimation of source dynamics. The results are visualized individually for each subject dataset. Last, the performance of the method is evaluated by VAF, and lateralization index and activation complexity are used to exam the difference of brain dynamic information flow for able-bodied and stroke participants. This section consists of 6 subsections: EEG preprocessing, the forward problem, the inverse problem, fiber tracking, dynamics estimation and model evaluation.

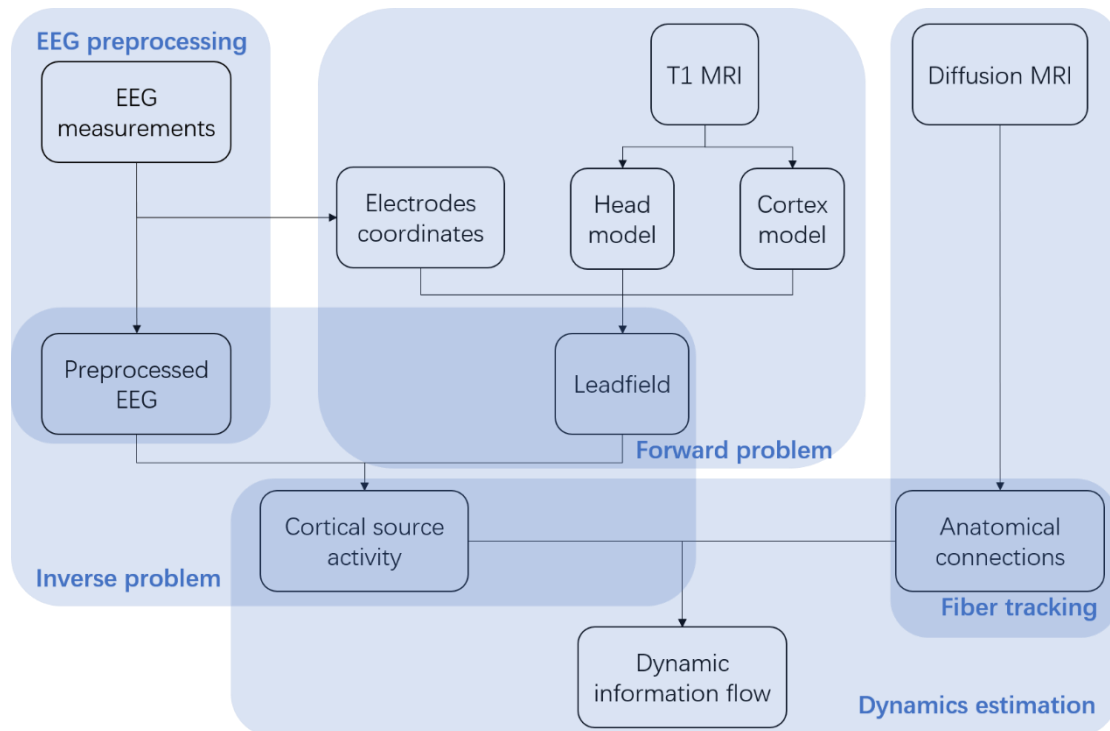


Figure 4 Workflow of the VBMEG method.

3.1 EEG preprocessing

EEG data were preprocessed using EEGLAB (Delorme and Makeig, 2004), which is an open source toolbox running in the MATLAB environment. Continuous EEG data was band-pass filtered between 1 and 30 Hz to remove possible slow trends in the data (e.g., blood pressure, heartbeat and breathing) and high-frequency fluctuations in event-related potentials, and then down-sampled to 512 Hz. EEG epochs were extracted using a window analysis time of 250ms, with 50ms before stimulus and 200ms after stimulus. The order of filtering and epoch extraction cannot be reversed, since applying filters on extracted epochs will cause aliasing. The artifact caused by electrical stimulus was removed by a blanking window from 10ms before the stimulus to 10ms after the stimulus. Then the gap was filled by a 3-order autoregressive model.

EEG epochs were re-referenced to a common average reference. According to Ohm's law, the outward positive and negative currents summed across an entire electrically isolated sphere (e.g. head) sum to zero. If we neglect the current passing through the base of the skull to the neck and body, we can assume that the sum of the electric field values recorded by all EEG electrodes is always 0. Then the average electric field is removed from each channel to re-reference EEG.

Independent Component Analysis (ICA) algorithm was used to remove the components of eye-blinks and movements. After the artifact removal, the baseline correlation was applied to each epoch using the signal from 50ms to 10ms before the stimulus. The epochs for the same experimental conditions were averaged in each subject, time-locked to the onset of the stimulus to extract the event-related potential (ERP).

Visualization of all electrode signals on the scalp can be achieved by topography. The activity of electrodes is plotted, by coding the strength in several tones of color (e.g. red depicts high EEG amplitude and blue depicts lower EEG amplitude). The spatial points lying between electrodes are calculated by interpolation, so that a smooth gradation of colors is achieved. We can view the pre-processing results intuitively from topographies.

3.2 The forward problem

The forward problem refers to calculate the potentials at the electrodes with a given electrical source. The leadfield matrix is constructed by integrating the influences of all sources to the electrodes. Solving the forward problem is necessary for source localization (the inverse problem), which is defined as estimating brain sources with measured potentials at the EEG electrodes. The boundary element method (BEM) (Mosher et al., 1999), which is a numerical technique for solving the forward problem, showed high accuracy in other researches and has the advantage of low computational needs. In BEM, a three-layer head model is built from surfaces, each encapsulating a tissue. The head model consists of brain-skull interface, skull-scalp interface and the outer surface. The regions between the interfaces are assumed to be homogeneous and isotropic conducting. Each interface is tessellated with boundary elements (triangles) to obtain a solution in such a homogenous volume.

In our research, an individual head model for each subject was built using the T1 MR image. A grey matter image was extracted from the T1 image using the SPM8 toolbox (Penny et al., 2011). Freesurfer (Reuter et al., 2012), a MRI processing software, was used to construct a polygon model of cortical surface, label the cortex surface anatomically, and extract the inner skull surface and outer scalp surface from the T1 image. **Figure 5** demonstrates three views of MR image segmentation. Then a three-layer (CSF, skull and scalp) head model was built using BEM by VBMEG toolbox.

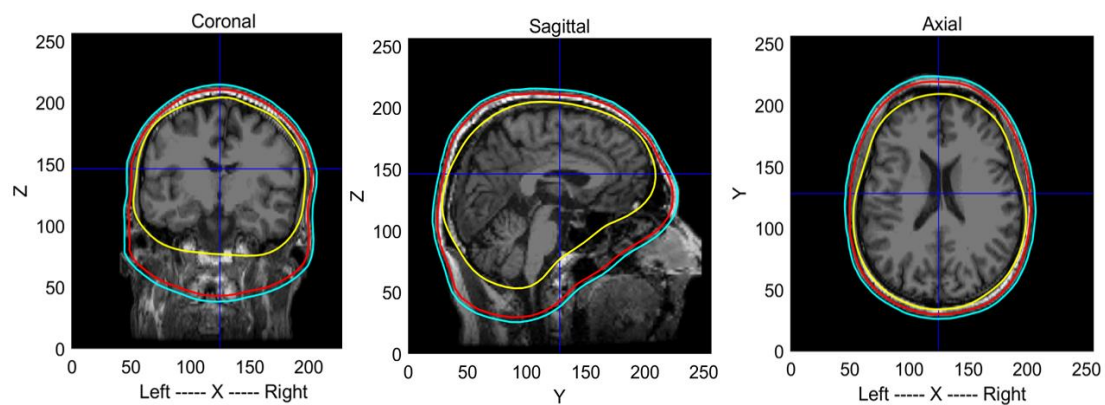


Figure 5 Three views of MR image segmentation. Yellow, red and cyan surface represents CSF, skull and scalp surfaces respectively.

10000 vertices on the cortex surface were chose as possible dipole sources, and the leadfield matrix was built based on the position of dipole sources and EEG electrodes, as well as the head model by VBMEG toolbox. The conductivity of CSF, skull and scalp was set as 0.62, 0.03 and 0.62 S/m respectively as the default setting in the toolbox.

3.2.1 Co-register EEG and MRI coordinates

EEG and MRI were measured separately, so that before combining these two neuroimaging methods together, we need to co-register EEG and MRI coordinates. During EEG experiment preparation, skull landmarks (e.g. preauricular and nasion) were positioned by 3D scanning as shown in **Figure 6**. These skull landmarks can also be found in T1-MRI as shown in **Figure 7**. Several software can select preauricular and nasion on T1-MRI automatically. However, the accuracy was shown to be low during our use. These skull landmarks were marked on T1-MRI manually by specialist. By aligning three non-coplanar points (left preauricular, right preauricular and nasion), we can co-register the EEG and MRI coordinates.

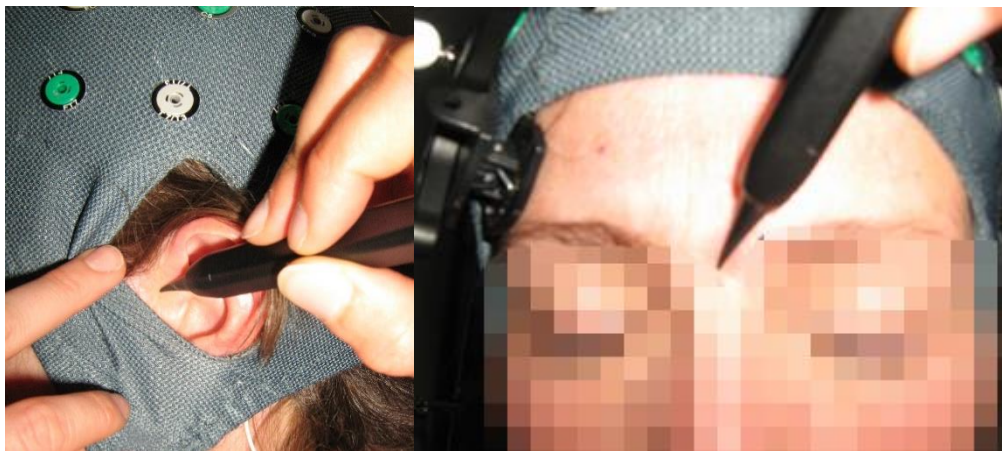


Figure 6 Positioning of preauricular and nasion during EEG experiment preparation. Face of the participant is pixelated for privacy protection.

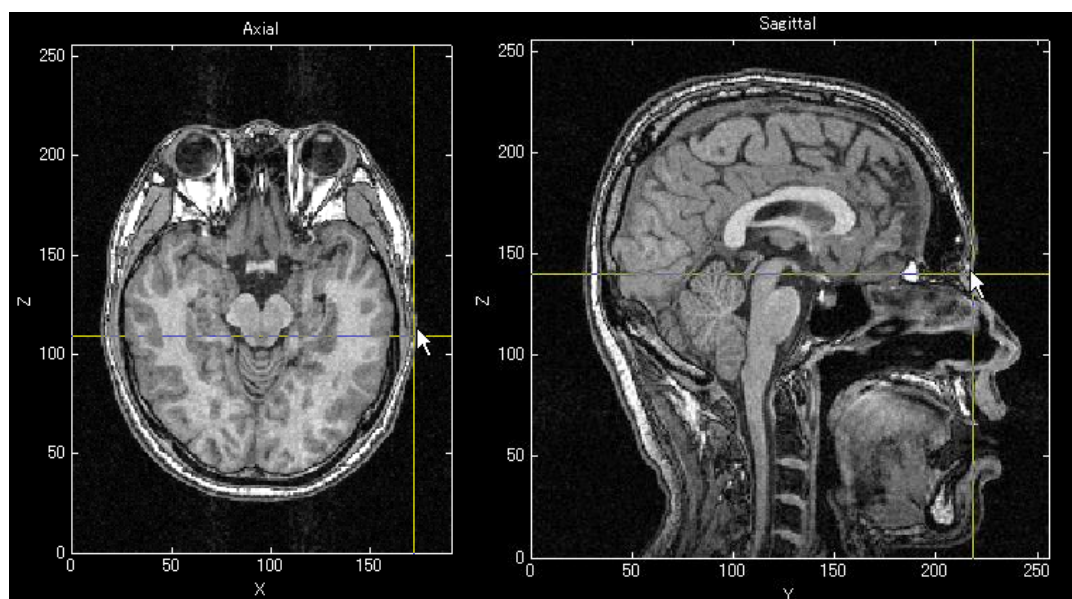


Figure 7 Positing of preauricular and nasion in T1-MRI

3.3 The inverse problem

The relationship between cortical source activities and EEG signals can be described as:

$$\mathbf{M} = \mathbf{L}\mathbf{S} + \mathbf{n} \quad 1$$

where \mathbf{M} is measured EEG signals, \mathbf{L} is the leadfield, \mathbf{S} is cortical dipole moments, and \mathbf{n} represents measurement noise. The inverse problem is to estimate the cortical source activities $\hat{\mathbf{S}}$, from the measured EEG signals as well as the leadfield built based on T1-MRI. Different from common linear regression problems, the inverse problem is an ill-posed problem (Baillet and Garnero, 1997), since the number of cortical sources is much larger than that of EEG electrodes, which allows infinite solutions of $\hat{\mathbf{S}}$. Distributed source approaches with additional constraints or prior information, e.g. minimum L2 norm regularization (MNE), spatial smoothness priors (LORETA), etc. showed promising results on both simulated and experimental data (Grech et al., 2008). Particularly, one advanced distributed source approach named hierarchical Variational Bayesian (hVB) method performs better than conventional methods as shown in previous researches (Sato et al., 2004). Thus, the hVB method was applied to estimate the source activities in our research.

Distributed source approach is established based on the Bayesian framework. According to the Bayes' Law,

$$P(\mathbf{S}|\mathbf{M}) = \frac{P(\mathbf{M}|\mathbf{S})P(\mathbf{S})}{P(\mathbf{M})}$$

where | means 'event conditional on', $P(\mathbf{S}|\mathbf{M})$ is the posterior probability, $P(\mathbf{M}|\mathbf{S})$ is the likelihood, $P(\mathbf{S})$ is the prior probability and $P(\mathbf{M})$ stands for model evidence. In common distributed source approaches, the goal is to find out a physically plausible estimator $\hat{\mathbf{S}}$, which provides maximum a posteriori (MAP), given the measured EEG signal \mathbf{M} . Thus, the estimator can be written as:

$$\hat{\mathbf{S}} = \max_{\mathbf{S}} P(\mathbf{S}|\mathbf{M}) \quad 2$$

If the posterior density of active sources $P(\mathbf{S}|\mathbf{M})$ is assumed to have a Gaussian distribution, we find

$$P(\mathbf{S}|\mathbf{M}) = \frac{P(\mathbf{M}|\mathbf{S})P(\mathbf{S})}{P(\mathbf{M})} = \frac{e^{-F_{\lambda}(\mathbf{S})}/z}{P(\mathbf{M})}$$

where z is a normalization constant called the partition function and $F_{\lambda}(\mathbf{S}) = U(\mathbf{S}) + \lambda D(\mathbf{S})$. $U(\mathbf{S})$ and $D(\mathbf{S})$ represent the energy function associated with $P(\mathbf{M}|\mathbf{S})$ and $P(\mathbf{S})$ respectively, and λ is a weighting factor. Then Equation (2) can be written as:

$$\hat{\mathbf{S}} = \min_{\mathbf{S}} F_{\lambda}(\mathbf{S}) = \min_{\mathbf{S}} (U(\mathbf{S}) + \lambda D(\mathbf{S})) \quad 3$$

If we assume the measurement noise \mathbf{n} is identically and independently distributed Gaussian noise with zero mean and has the same variance σ_n for each electrode, we can write the probability distribution function of \mathbf{n} as:

$$P(\mathbf{n}) = \frac{1}{\sigma_n \sqrt{2\pi}} e^{-\frac{|\mathbf{n}|^2}{2\sigma_n^2}}$$

where σ_n is typically determined from pre-stimulus rest period measurements and $|\cdot|^2$ represents L2 norm. Since the linear relationship in Equation (1) holds, the probability distribution of the measurements M with given cortical source activities \mathbf{S} follows:

$$P(\mathbf{M}|\mathbf{S}) \propto e^{-\frac{|\mathbf{M}-\mathbf{L}\mathbf{S}|^2}{2\sigma_n^2}}$$

So, we can write the energy term $U(\mathbf{S})$ associated with $P(\mathbf{M}|\mathbf{S})$ as:

$$U(\mathbf{S}) = |\mathbf{M} - \mathbf{L}\mathbf{S}|^2$$

There are many ways to define the energy term $D(\mathbf{S})$ associated with $P(\mathbf{S})$. The hierarchical Variational Bayesian (hVB) method introduced a hierarchical prior. First, we can assume the cortical source current follows Normal distribution, which gives:

$$P(\mathbf{S}_{1:T}|\boldsymbol{\alpha}) \propto \exp\left(-\frac{1}{2} \sum_{t=1}^T \mathbf{S}(t)' \cdot \mathbf{A} \cdot \mathbf{S}(t)\right)$$

where \mathbf{A} is the diagonal matrix with diagonal elements $\boldsymbol{\alpha} = [\alpha_n | n = 1:N]$. We also assume that the current variance $\boldsymbol{\alpha}^{-1}$ does not change over period T . The energy term $D(\mathbf{S})$ is defined as:

$$D(\mathbf{S}) = \mathbf{S}' \cdot \mathbf{A} \cdot \mathbf{S}$$

where Σ_0 is an activity dependent inverse covariance matrix. Combining the defined energy term $U(\mathbf{S})$ and $D(\mathbf{S})$ with Equation (3), we get:

$$\hat{\mathbf{S}} = \min_{\mathbf{S}} (U(\mathbf{S}) + \lambda D(\mathbf{S})) = \min_{\mathbf{S}} (|\mathbf{M} - \mathbf{L}\mathbf{S}|^2 + \lambda \mathbf{S}' \cdot \mathbf{A} \cdot \mathbf{S})$$

The hVB method considers the current variance as unknown parameters and uses measured EEG data to estimate the current variance by introducing a hierarchical prior. the current inverse variance parameter $\boldsymbol{\alpha}$ is estimated by introducing an Automatic Relevance Determination (ARD) hierarchical prior:

$$P(\boldsymbol{\alpha}) = \prod_{n=1}^N \Gamma(\alpha_n | \bar{\alpha}_n, \gamma_{0n} \alpha_n)$$

$$\Gamma(\boldsymbol{\alpha} | \bar{\boldsymbol{\alpha}}, \boldsymbol{\gamma}) \equiv \boldsymbol{\alpha}^{-1} \left(\frac{\boldsymbol{\alpha}\boldsymbol{\gamma}}{\bar{\boldsymbol{\alpha}}}\right)^{\boldsymbol{\gamma}} \Gamma(\boldsymbol{\gamma})^{-1} e^{-\boldsymbol{\alpha}\boldsymbol{\gamma}/\bar{\boldsymbol{\alpha}}}$$

where $\Gamma(\boldsymbol{\alpha} | \bar{\boldsymbol{\alpha}}, \boldsymbol{\gamma})$ represents the Gamma distribution with mean $\bar{\boldsymbol{\alpha}}$ and degree of freedom $\boldsymbol{\gamma}$. $\Gamma(\boldsymbol{\gamma}) \equiv \int_0^{\infty} dt t^{\boldsymbol{\gamma}-1} e^{-t}$ is the Gamma function. This hierarchical prior gives nonzero probabilities for any value of the inverse variance parameter α_n , instead of a constant value based on prior information in conventional normal prior. The inverse variance parameter α_n keeps updating until converge during the estimation, and this decreases the influence of possible false prior information.

Besides the hierarchical prior on current variance, hVB method contains a smoothness prior, which enforces high correlations between neighboring current activity. Mathematically, the smoothness prior is imposed as the structural constraint on the off-diagonal part of the covariance matrix:

$$P(\mathbf{S}_{1:T}|\boldsymbol{\alpha}, \boldsymbol{\beta}) \propto \exp\left[-\frac{1}{2} \sum_{t=1}^T \mathbf{S}'(t) \cdot \boldsymbol{\Sigma}_{\alpha} \cdot \mathbf{S}(t)\right]$$

where the current covariance matrix $\boldsymbol{\Sigma}_{\alpha}^{-1}$ is given by:

$$\boldsymbol{\Sigma}_{\alpha}^{-1} = \mathbf{A}^{-1} + \mathbf{W} \cdot \boldsymbol{\Lambda}^{-1} \cdot \mathbf{W}' \quad 5$$

\mathbf{A} and $\boldsymbol{\Lambda}$ are the diagonal matrices with the diagonal elements $\boldsymbol{\alpha} = [\alpha_n | n = 1:N]$ and $\boldsymbol{\beta} = [\beta_n | n = 1:N]$ respectively and \mathbf{W} is the smoothing filter. The first and second term in the r.h.s. of Equation (5) controls the diagonal and diagonal part of the current covariance matrix respectively. As the variance parameter α_n^{-1} increases, the variance of the n th current increases; as the smoothness parameter β_n^{-1} increases, the correlation between the n th and the neighboring currents increases. The smoothing filter \mathbf{W} can be defined based on prior assumption. If we assume the Gaussian smoothing filter of \mathbf{W} , the correlation in the current activity between two points decreases exponentially as the squared distance increases.

The relationship between the cortical source currents and EEG measurements is indicated by Equation (1). By introducing the Bayesian framework, the estimation tries to find physically plausible source currents, which can maximize a posterior, as indicated by Equation (2). The hierarchical Variational Bayesian (hVB) method involves a hierarchical prior on source current variance as well as a smoothness constraint on neighboring source currents. The hVB method is established on the following assumptions:

1. The posterior density $P(\mathbf{S}|\mathbf{M})$ is assumed to follow Gaussian distribution.
2. The measurement noise n is identically and independently distributed Gaussian noise with zero mean and has the same variance σ_n for each electrode
3. The cortical source current $P(\mathbf{S})$ follows Normal distribution.
4. The variance of the source current follows Gamma distribution.
5. The smoothing filter \mathbf{W} on the source current can be assumed as a Gaussian smoothing filter.

Assumption 1, 2 and 3 are common in distributed source approach. Assumption 5 is usually applied in the method with spatial constraints. Assumption 4 is introduced by the hVB method for the first time to decrease the negative influence of possible false prior information on current variance. Since the presence of hierarchical prior, conventional linear inverse is not applicable, so that Variational Bayesian method is used.

In our research, the source activity was estimated with pre-processed EEG signals and estimated leadfield matrix using hVB method, which is implemented in the VBMEG toolbox.

3.4 Fiber tracking

The estimation of dynamic information flow is constrained by the existence of anatomic connections among regions of interests (ROIs). The cortical surface was parcellated into 250 target ROIs with the centers equally distributed on the cortex surface. The remaining cortex vertices were clustered into these ROIs based on their spatial proximity. Anatomic connectivity information was achieved from diffusion-weighted imaging (DWI). Diffusion MRI maps the diffusion processes of molecules, by measuring their motion after being applied a huge magnetic field. In an isotropic medium, water molecules move randomly, while in biological tissues, the molecules move principally along the axis of the neural fiber. If the molecules in a particular voxel diffuse principally in one direction, we can assume the majority of the fibers in this area are parallel to that direction. In DWI, the diffusion is measured in multiple directions, so that the anatomic connectivity of different regions in the brain can be examined.

The dMRI data were preprocessed using FSL v5.0 (<http://fsl.fmrib.ox.ac.uk/fsl/>) (Jenkinson et al., 2012). The acquired DWIs were corrected for motion and eddy current distortion by affine co-registration to the reference b0-image (using FSL `eddy_correct`). Gradient directions were reoriented according to the rotation component of the affine transformation. Diffusion tensor fitting and fractional anisotropy (FA) were calculated using FSL, and fiber tracking was performed with MRTrix software v0.2.10 (<http://jdtournier.github.io/mrtrix-0.2/index.html>).

The fiber tracking results provide information about the presence of fiber connections between ROIs as well as the length of the fibers. The time lags in the MAR model were estimated based on the length of fiber connection using the theoretical conduction velocity of axon equal to 6 m/s (Fukushima et al., 2015). **Figure 8** gives an example of fiber tracking results of a control participant.

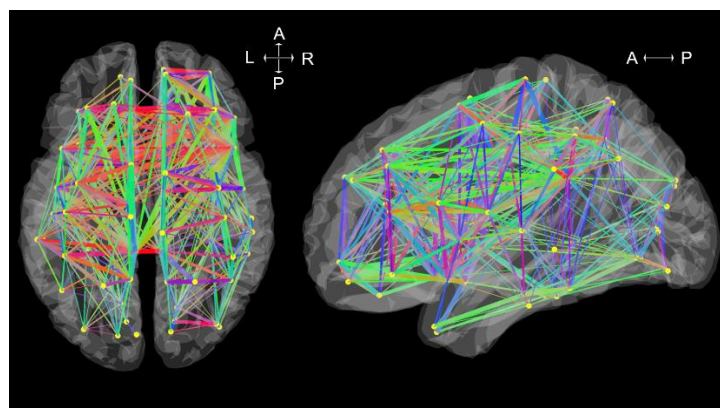


Figure 8 Fiber tracking results of a control participant. The yellow dots represent centers of ROIs, and the lines represent fibers connecting ROIs.

3.5 Dynamic information flow estimation

The dynamic information flow was estimated by a multivariate autoregressive (MAR) model to determine whether causal interactions exist between active cortical sources. The implantation of MAR model is based on the theory of Wiener-Granger Causality (WGC). The basic idea of WGC is that, if a signal $x_1(t)$ contains information in the past that can help estimate the signal $x_2(t)$, then $x_1(t)$ is said to cause $x_2(t)$. If we assume the interactions between ROIs are linear, we can get the MAR model:

$$\mathbf{X}_t = \sum_{k=1}^P \mathbf{A}_k \mathbf{X}_{t-k} + \epsilon_t$$

where \mathbf{X}_t is the state vector consists of activity of sources at certain time, p denotes the order of the process, and ϵ_t is multivariate white noise. The matrices \mathbf{A}_k are the auto-regression (AR) coefficients because they regress \mathbf{X}_t onto its own past. The MAR model can be considered as a linear combination of the most recent past p values. This property shows that MAR model is a quantified presentation of the WGC between ROIs. The AR coefficients can be estimated by L2-regularized least squares method, which is solved by finding the matrices \mathbf{A}_t that minimize the estimated innovation variance:

$$\mathbf{E}^{\text{LIN}} = \sum_{t=1}^{N_t} \left(\mathbf{X}_t - \sum_{k=1}^P \mathbf{A}_k \cdot \mathbf{X}_{t-k} \right)^2$$

One limitation of conventional MAR model is that non-zero AR coefficients can be estimated between ROIs without anatomical connectivity. Thus, in our research, an anatomical constraint was applied to the MAR model based on the fiber tracking results from diffusion MRI, so only the anatomically connected sources have the non-zero weights. Source activity of ROIs was calculated as the mean of contained dipole moments. Then, source activity of these 250 ROIs were defined as the variables in MAR model. The time lags in the MAR model were estimated based on the length of fiber connection using the theoretical conduction velocity of axon equal to 6 m/s (Fukushima et al., 2015). For each pair of estimated sources, it was determined if the direct anatomic connection exists. If there was no connection, then the coefficients of the AR model between these two sources were put to zero. If the connection existed, then a time delay was calculated. Only the coefficients corresponding to this time lag between these two sources would be non-zero. Thus, only one order of the AR model could be non-zero and the MAR model could be represented by a two-dimensional matrix. Self-influence of each source was assumed to only have the second order. Mathematically, the MAR model with anatomical constraint can be described by:

$$s_{n,t} = \sum_{d=1}^p a_{nd} \cdot s_{n,t-d} + \sum_{v \in \mathcal{C}_n} b_{nv} \cdot s_{v,t-\Delta_{vn}} + \epsilon_n$$

where $s_{n,t}$ is the current density at time t of ROI n , a_{nd} is the local dynamics

parameters, p is the self-influence AR order which is assumed to be 2, b_{nv} is the distant interaction parameters, C_n is an index set of structurally connected ROIs with ROI n , and u_n is white noise. Δ_{v_n} is defined as $\frac{L_{v,n}}{c} + D$, where $L_{v,n}$ is the fiber length connecting ROI n and m , c is the conduction velocity and D is the synaptic delay which is assumed to be 20s. The MAR weights were estimated based on fiber connections and their corresponding time lag using an L2-regularized least-squares method.

3.6 Model evaluation

The performance of source localization and dynamic information flow estimation was evaluated by calculating the Variance Accounted For (VAF). VAF is used to verify the correctness of a model, by comparing the real signal with the estimated output of the model. The VAF of two same signals is 100%, and the more different of the signals the lower the VAF. For source localization, the estimated sources \hat{S} were used to generate an estimated EEG signal $\hat{M} = L\hat{S}$, which was compared with collected EEG signal M . For the i th EEG channels, VAF_{M_i} was defined as:

$$VAF_{M_i} = \left(1 - \frac{\text{var}(M_i - \hat{M}_i)}{\text{var}(M_i)} \right) \cdot 100\%$$

The time window was chosen as from 0ms to 200ms. The VAF for source localization VAF_M was defined as the median of VAF_{M_i} for all EEG channels. With a specific stimulus, only parts of the brain sources are activated, which means the amplitude of different EEG channels is different as well. When the signal amplitude is lower, the signal to noise ratio (SNR) is lower and the upper boundary for VAF is lower as well. Under this scenario, the mean of VAF_{M_i} cannot evaluate the performance of the model correctly. Thus, median of VAF_{M_i} was chosen to represent the performance of source localization.

For dynamic information flow estimation, one step forward (2ms) of source activity \hat{S} was estimated by the MAR model. The estimated source activity was compared with the results S from source localization. For a specific time point t , the $VAF_S(t)$ was defined as:

$$VAF_S(t) = \left(1 - \frac{\text{var}(S(t) - \hat{S}(t))}{\text{var}(S(t))} \right) \cdot 100\%$$

where $S(t)$ and $\hat{S}(t)$ are vectors containing all source activities resulting from source localization and estimated from MAR model respectively, and t is the time going from 0ms to 200ms. The VAF for dynamic information flow VAF_S was defined as the mean of $VAF_S(t)$ in the time window.

As the accuracy of the MAR model can be affected by the signal to noise ratio, the signal to noise ratio of the EEG recording was also calculated. The SNR is defined as follows:

$$SNR = \frac{A_{RMS_{signal}}}{A_{RMS_{noise}}}$$

where A_{RMS} is the root mean square amplitude. To intuitively show the signal level, signal percentage was calculated by

$$P_{signal} = \frac{A_{RMS_{signal}}}{A_{RMS_{signal}} + A_{RMS_{noise}}} \cdot 100\%$$

The brain dynamic information flow difference between control and stroke participants are evaluated by two metrics: lateralization index and activation complexity. Lateralization index indicates the hemispheric dominance. If the stimulus was performed on the right hand, lateralization index is calculated as:

$$LI = \frac{D_{\text{left}} - D_{\text{right}}}{D_{\text{left}} + D_{\text{right}}}$$

where D_{left} and D_{right} are the number of ROIs, whose outward information flow strength is above the median z-score, in the left and right hemisphere respectively. The outward information flow strength is defined as the source activity times the sum of absolute AR coefficients starting from this ROI. Lateralization index is between -1 and 1. If it is 1, the contra-stimulus hemisphere is in dominant; while if it is -1, the ipis-stimulus hemisphere is in dominant.

Activation complexity implies percentage of active fibers among all fibers which connect ROIs. It is defined as:

$$AC = \frac{N_{\text{active fibers}}}{N_{\text{connections}}}$$

where $N_{\text{active fibers}}$ is the number of fibers, whose corresponding AR coefficient is above the median z-score. $N_{\text{connections}}$ is the number of all anatomical connections. Activation complexity is a ratio between 0 and 1. The larger the activation complexity, the more fibers are activated post stimulus.

4 Results

The results of the method application are illustrated in four cases: for two able-bodied individuals and two chronic stroke subjects.

In **Figure 9** the ERP of a control and a stroke subject are presented. In line with the literature (Wang et al., 2016, Oniz et al., 2016), a positive-going peak around 50 ms (P50) and a negative-going peak around 100 ms (N100) were identified in the ERP for both control and stroke. Additionally, we provide the ERP topographies at the latency of P50 in **Figure 10**. Both controls have similar topographies with large ERP values at the sensorimotor area of the contralateral hemisphere. This result is consistent with previous studies (Buchner et al., 1995, Desmedt and Cheron, 1980, Druschky et al., 2003). Individual differences are shown in stroke patients, which may be related to subject-specific lesion load and recovery.

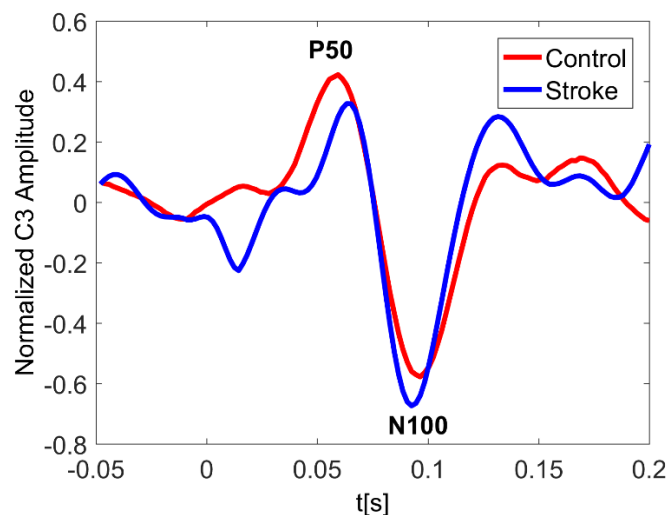


Figure 9 Normalized C3 Amplitude for typical control and stroke participant with stimulus on right hand. The ERP plotting at electrode C3 shows great similarity for both control and stroke. The latency of P50 peak for stroke is slightly larger than that of control.

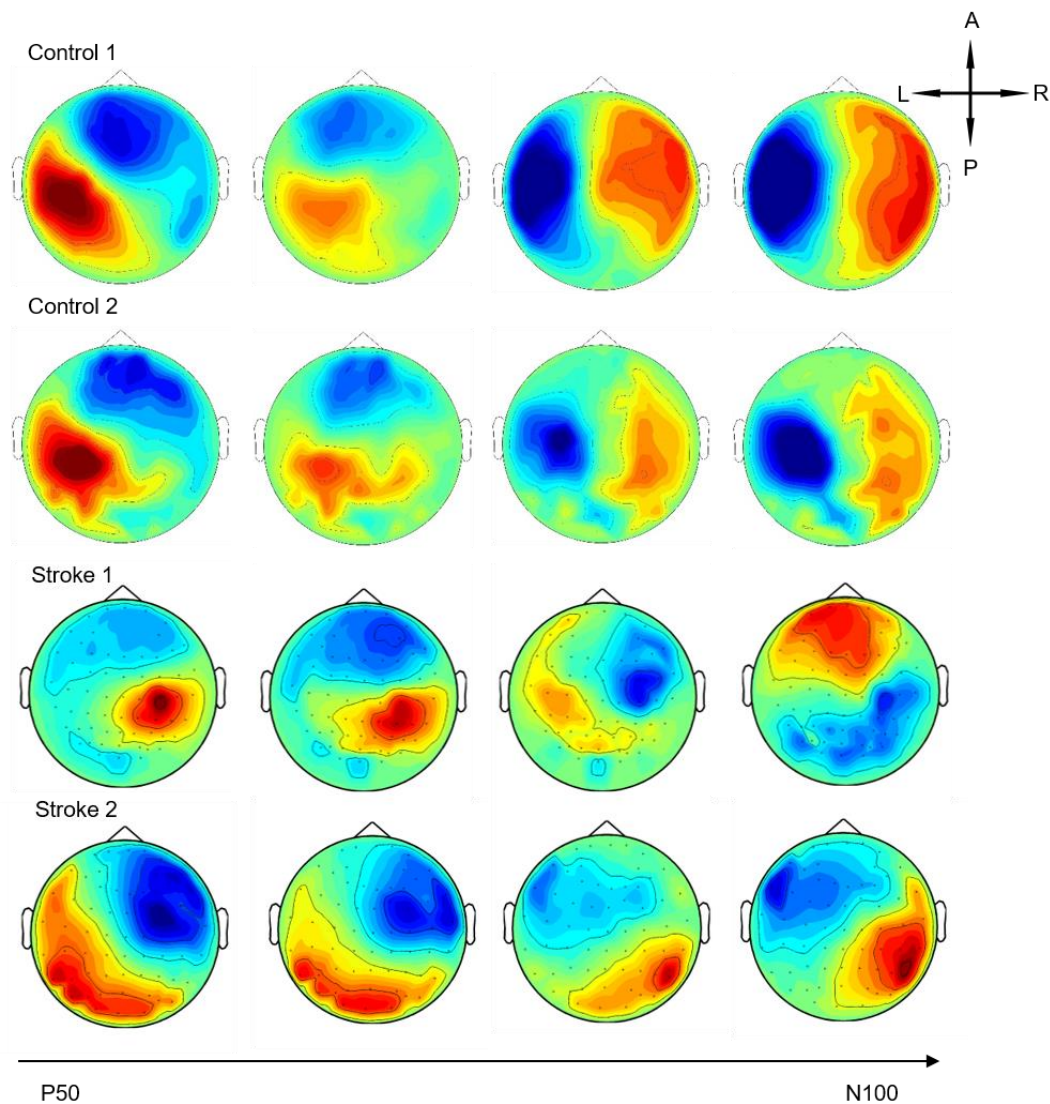


Figure 10 Topographies from 50ms to 100ms (left to right). Stimulation was applied on left hand for stroke 1 and on right hand for the rests.

The VAF of EEG source localization is shown in **Table 2**, where we can see the VAF of source localization is higher than 80 % for all subjects. **Figure 11** 错误!未找到引用源。 shows the estimated dynamic information flow for each subject with finger stimulation at the dominant hand for control subjects, and at the affected hand for stroke participants. It also schematically depicts the anatomic connections between the active sources. The information flow is shown only at the contralateral hemisphere in the control subjects, while at the both hemispheres in the stroke participants. In the time period between P50 and N100 peaks, information flow occurs in the ipsilateral (contralesional) hemisphere, i.e. the left hemisphere for stroke subject 1 and the right hemisphere for stroke subject 2.

Subject	VAF, Right Hand	VAF, Left Hand
Control 1	94.49 %	96.28 %
Control 2	93.64 %	92.27 %
Stroke 1	90.03 %	87.12 %
Stroke 2	85.63 %	83.79 %

Table 2 The VAF of EEG source localization (inverse problem) for each subject.

The VAF of dynamic information flow estimation is provided in **Table 3**, where the VAF is higher than 90% for all subjects. Additionally, we also provide the SNR for all subjects in **Table 4**. Although the SNR for the stroke subjects is slightly lower than the controls, the signal percentage is above 88% for all subjects. To determine the baseline value of VAF when the input signal of the model is random, we replaced ERP signals with white noise. The same estimation and prediction process was repeated 100 times with different noise realizations to determine the baseline. The estimated VAF obtained from this baseline test was around zero. Therefore, the high VAF from our dynamic information flow estimation on the EEG source activity can prove the significance of our results by comparing with this baseline.

Subject	VAF Right Hand		VAF Left Hand	
	mean	std	mean	std
Control 1	97.77 %	12.42 %	97.77 %	12.41 %
Control 2	97.58 %	10.00 %	97.78 %	12.42 %
Stroke 1	92.30 %	14.80 %	93.75 %	12.06 %
Stroke 2	91.69 %	11.58 %	92.86 %	10.47 %

Table 3 The average VAF for dynamic estimation with standard deviation.

Subject	Right Hand		Left Hand	
	SNR (dB)	Signal percentage	SNR (dB)	Signal percentage
Control 1	14.22	96.35 %	13.76	95.97 %
Control 2	13.45	95.68 %	15.28	97.12 %
Stroke 1	7.64	85.30 %	8.62	87.92 %
Stroke 2	9.92	90.76 %	8.71	88.13 %

Table 4 Signal to noise ratio in each subject when the corresponding hand was stimulated. In Stroke 1 case left hand was impaired. In Stroke 2 case right hand was impaired.

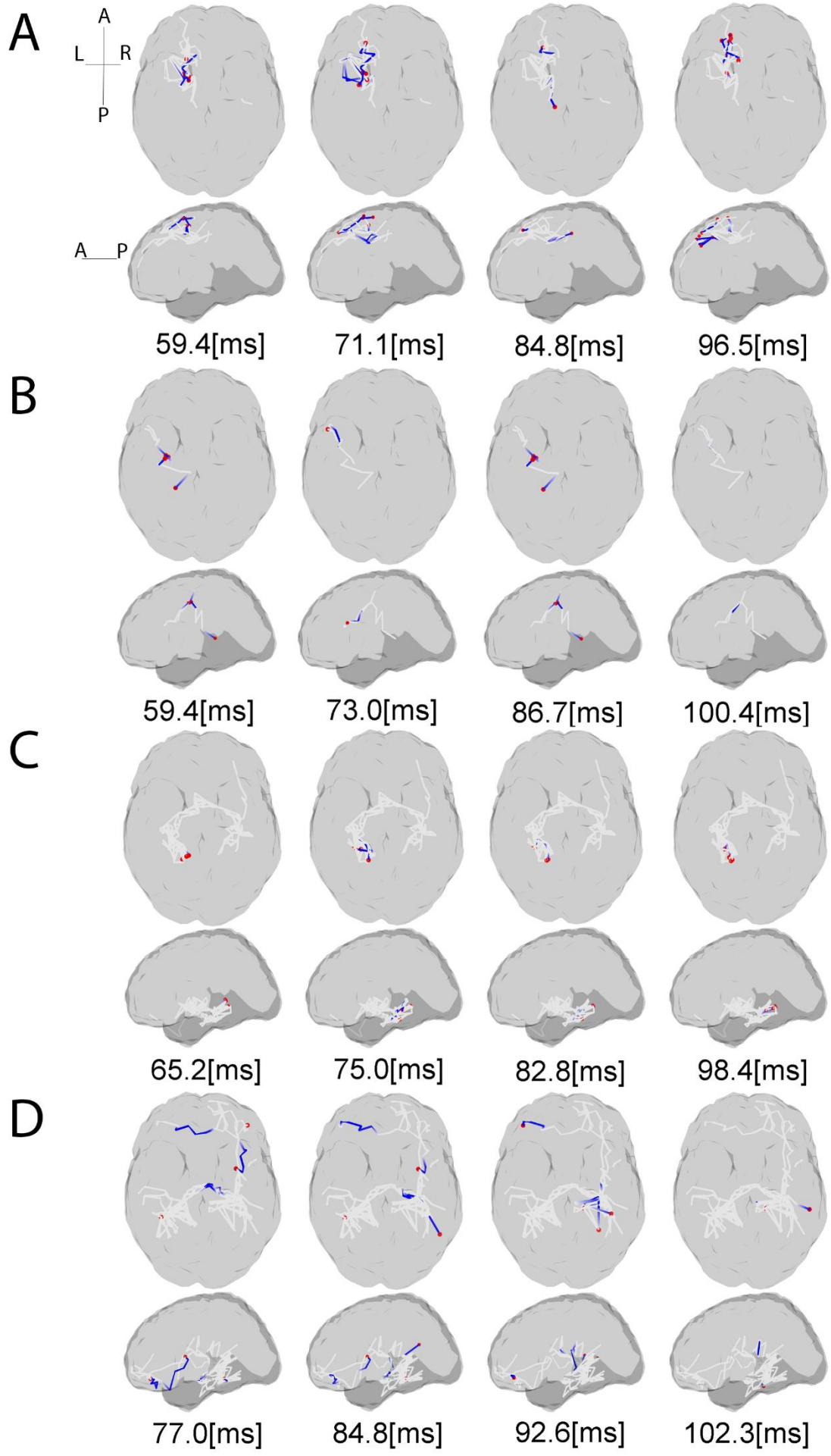


Figure 11 Source interactions estimated from MAR model. The plots show the information flow between P50 and N100 for each subject and anatomic connections between the active sources estimated via white matter tractography based on the individual dMRI acquisitions. The gray lines indicate the whole fiber network involved in the transmission of somatosensory information flow through the brain. The blue lines show the currently active fibers, and red dots are the currently active sources on the cortex at the specific time points. The ‘active sources’ here denotes the sources have electrical neural activities at the presented time point, while ‘active fibers’ indicate the fibers where the information flow is travelling through. For each subject projection of all axial slices (top) and of all sagittal slices (bottom) are shown. (A-B): controls, (C): stroke 1, (D): stroke 2.

For each subject, estimated coefficients matrices of the MAR model are presented in **Figure 12**, where we can see that increased inter-hemisphere interactions are shown for the stroke participants. This increase is also characterized by the number and percentage of the non-zero LCD model coefficients within and between hemispheres as shown in **Table 5**.

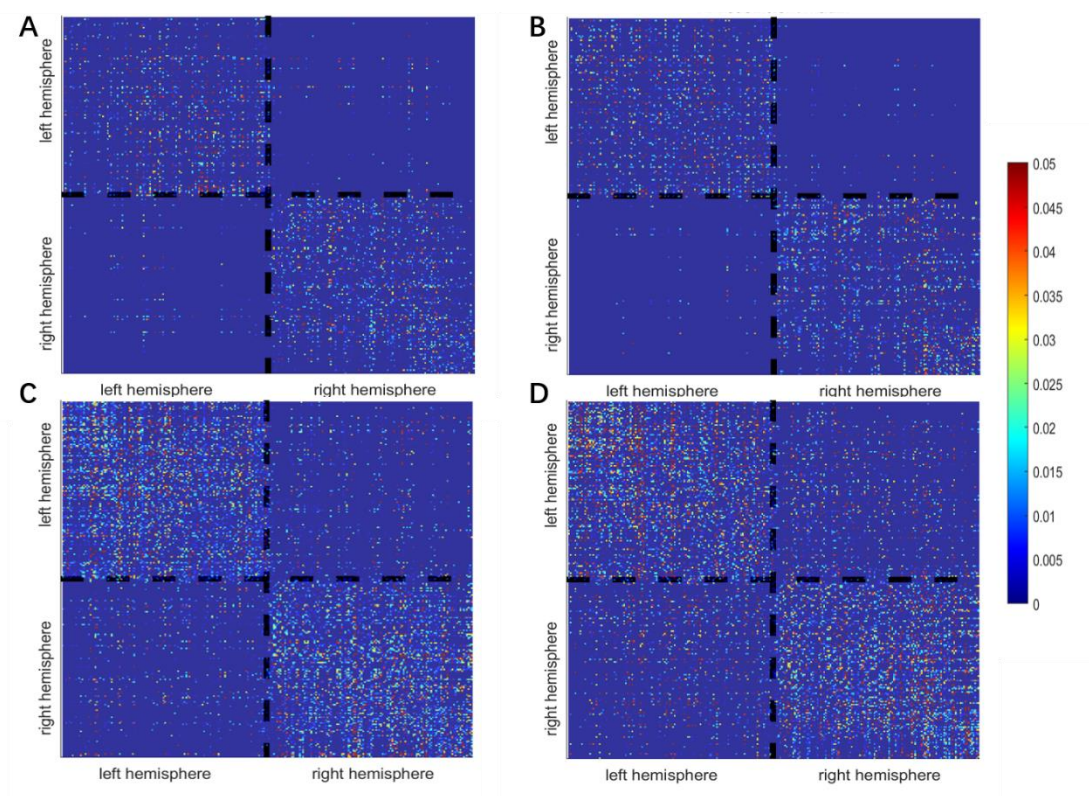


Figure 12 Estimated AR coefficient matrices for control and stroke participants (effective connectivity). (A-B): controls, (C): stroke 1, (D): stroke 2.

	intra-hemispheric interactions		inter-hemispheric interactions	
	Number of interactions	Percentage	Number of interactions	Percentage
Control 1	4956	89.3%	594	10.7%
Control 2	4930	93.51%	342	6.49%
Stroke 1	11868	84.18%	2230	15.82%
Stroke 2	11274	76.51%	3462	23.49%

Table 5 Number and percentage of intra-hemispheric vs. inter-hemispheric interactions represented by non-zero MAR model coefficients.

To illustrate how the anatomical priors used in VBMEG improves the estimation of dynamic information flow, we also used a conventional method based on correlation metrics (Greicius et al., 2003) to estimate brain functional connectivity without involving anatomical constraints. As shown in 错误!未找到引用源。 , numerous spurious connectivity was estimated between the sources, for which there is no physical pathway connection. It is also quantified in **Table 6** as the number of false positives and false discovery rate.

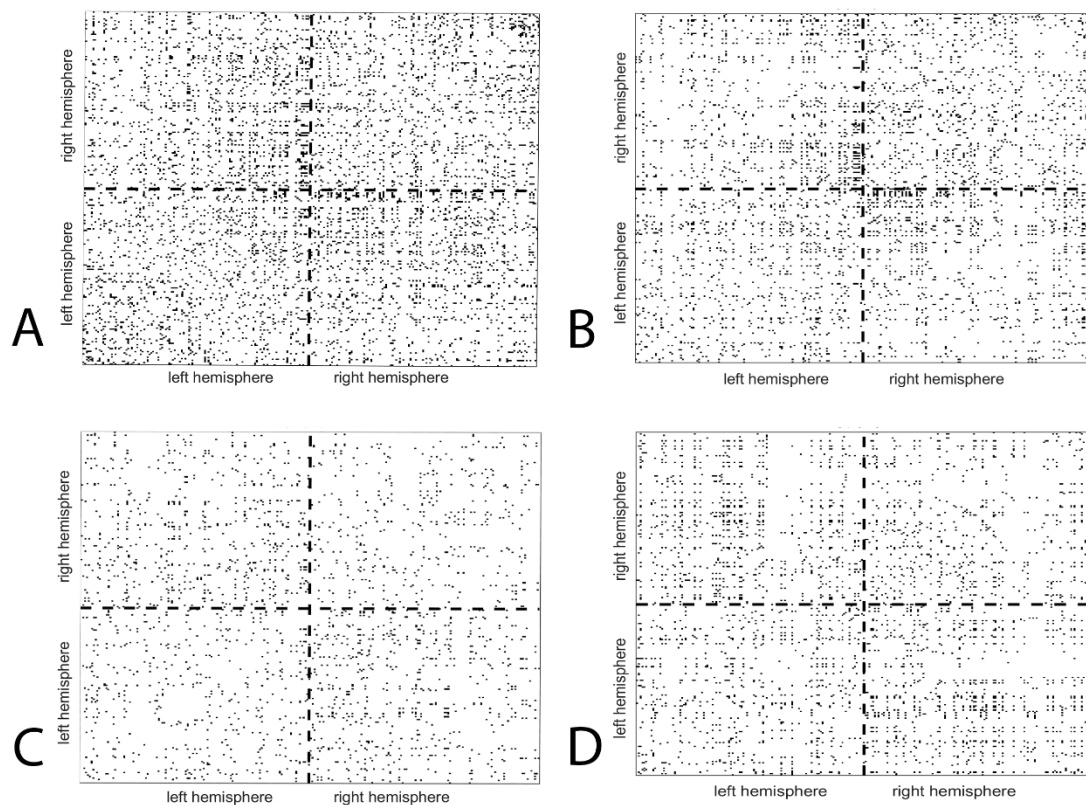


Figure 13 False positives (indicated by the black dots in the maps) of functional connectivity generated by correlation metrics compared to effective connectivity in which also the anatomical connectivity is taken into account. (A-B): controls, (C): stroke 1, (D): stroke 2.

	Number of false positives	False discovery rate
Control 1	5342	49.05 %
Control 2	3598	40.56 %
Stroke 1	2084	12.88%
Stroke 2	2896	16.42%

Table 6 Number of false positives (FP) and false discovery rate, i.e. $FP / (FP + TP) \times 100\%$, generated by correlation metrics without involving anatomical constraints. TP: True positive.

The lateralization index for each is shown in **Figure 14**. For control participants, the lateralization index is around 0.45, which indicates the contra-stimulus hemisphere is in dominant. The lateralization index for stroke participants is between -0.4 and -0.2, which indicates the ipsi-stimulus hemisphere is activated slightly higher than contra-stimulus hemisphere.

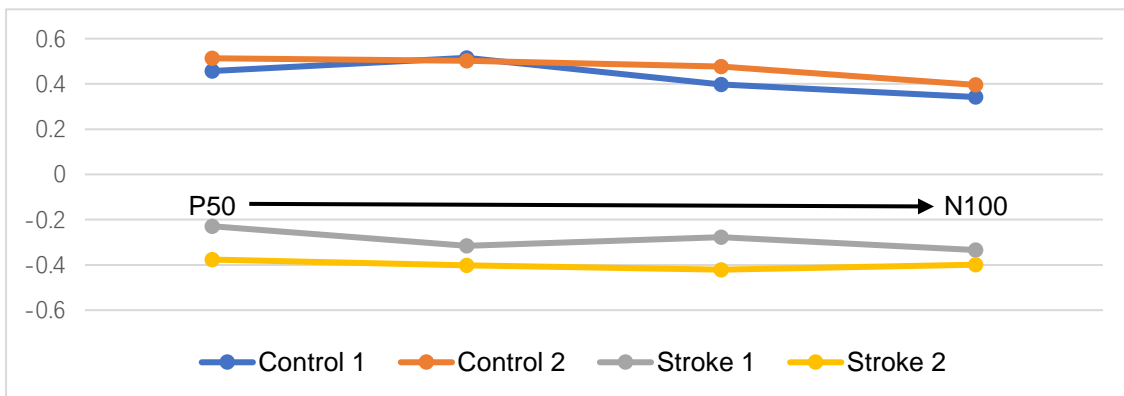


Figure 14 Lateralization index for each subject from P50 to N100.

The activation complexity for each subject is shown in **Table 7**. For able-bodied participants, around 30% fibers are activated, while for stroke participants, the number of activation fibers is doubled.

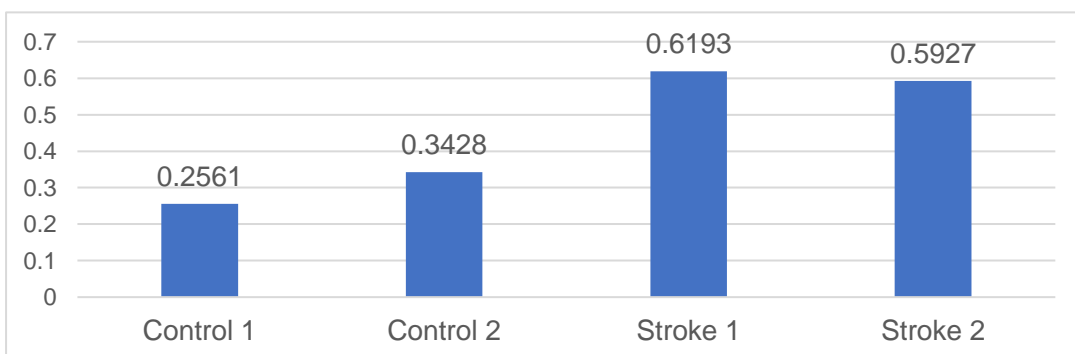


Table 7 Activation complexity for each subject

5 Discussion

The present work serves for two aims: first is to test the two-stage estimation procedure of the VBMEG method, consisting of an estimation of EEG sources and a dynamic estimation of the information flow between them; second, application of the VBMEG method gives a visualization of brain dynamic information flow for both able-bodied and stroke participants and their difference is compared quantitatively. Application of the VBMEG method as well as the metrics fills the gap that conventional clinical tests cannot take insight brain function changes after a stroke.

The estimation of information flow between sources, which is achieved by modeling a dynamic MAR model, provides insight on functional integration between brain areas. By including diffusion MRI information, only the sources having the anatomical connection are included in the estimation of dynamic information flow, which controls the type I error in the MAR modeling. In the VBMEG method, assumptions were made regarding the spatial sparseness and smoothness of the currents, as well as regarding the noise distribution being Gaussian and temporally uncorrelated. The performance of EEG source localization and MAR modeling was assessed by the variance accounted for (VAF) (Vlaar et al., 2017, Kalogianni et al., 2018b). The VAF is a summary of how much of the variability of the data can be explained by a fitted model. High VAF for both source localization and MAR modeling was reported in all tested datasets, indicating the VBMEG method can precisely capture the task-relevant cortical source activity and the dynamics in the brain network. The visualization of brain dynamic information flow gives an intuitive demonstration how brain areas influence each other. Besides the visualization, lateralization index indicates hemiparetic dominance for able-bodied and stroke participants quantitatively. Activation complexity shows the significant difference of active fibers for able-bodied and stroke participants.

In terms of stroke research, many efforts have been previously made to develop advanced methods based on fMRI to investigate reorganization of the sensorimotor system following a stroke. However, the poor temporal resolution of fMRI limits its ability to capture fast somatosensory information flow between cortical regions, which typically occurs in less than a hundred milliseconds. Therefore, a dynamic method based on EEG is highly desired for studying stroke. Most existing methods computing EEG source interactions are based on signal correlation/coherence (Srinivasan et al., 2007, Smit et al., 2008) or purely signal-driven MAR modelling (Baccalá and Sameshima, 2001, Kamiński et al., 2001, Blinowska et al., 2004, Bressler and Seth, 2011) without referring to anatomical pathways in the brain (Sakkalis, 2011, Friston, 2011b). When compared to a conventional method based on correlation metrics (Greicius et al., 2003), it is clear that our method combining the anatomic constraints provided a way to avoid spurious connectivity estimations.

For the able-bodied individuals, the estimated cortical sources and dynamic information flow are found only at the sensorimotor areas contralateral to the finger stimulation. This result is consistent with previous electro-neurophysiological studies (Jamali and Ross, 2013, Kalogianni et al., 2018a, Porcaro et al., 2013), showing that the somatosensory information is processed by brain regions predominantly contralateral to the stimulated hand. Conversely, in chronic hemiparetic stroke participants, the activation of brain activity occurs in both hemispheres, with information flow running through the ipsilateral (contralesional) hemisphere in the time period between P50 and N100. Our results provide evidence of reconfiguration of somatosensory cortical networks in individuals with hemiparetic stroke, which cannot be revealed by current clinical assessments. The reconfiguration of somatosensory cortical network may contribute to our understanding of time-dependent mechanisms during recovery of the sensory as well as motor function post hemiparetic stroke (Nelles et al., 1999, Ward, 2017). A better understanding of the recovery of somatosensory function is imperative as it serves as an essential feedback channel for the control of movement (Scott, 2004, Todorov and Jordan, 2002). Thus, the VBMEG has potential to evolve into a new neuroimaging tool to monitor cortical network changes post hemiparetic stroke and thus improving our understanding of stroke recovery.

This work presented a multi-modal brain imaging method which combines anatomical and physiological information from MRI and EEG. Different from conventional EEG connectivity methods that are purely based on mathematical modelling and signal correlation, our method considers physical connections between cortical sources (obtained from dMRI), which reduces the chance of false positive in the connectivity assessment. This allows for a comprehensive way to track neural information flow traveling between cortical regions through neural fibers. Moreover, compared to the fMRI-based connectivity methods, this EEG-dMRI combined method can provide a fine temporal resolution to capture fast somatosensory information flow in the brain, which occurs at the timescale in order of milliseconds.

Nevertheless, the current work has several limitations and could be improved in following directions:

- Ideally, the presented method could be configured in a way that simultaneously estimates EEG sources and dynamic information flow, known as “one-step” strategy (Fukushima et al., 2015). However, the implementation of one-step strategy has yet to be improved and validated¹. Therefore, in this study, we employed the “two-step” strategy where the EEG source localization and dynamic information were performed sequentially.
- Individual tissue conductivity and white matter conduction velocity could be better estimated in the future.

¹ http://vbmeg.atr.jp/docs/v2/static/vbmeg_users_manual.html#toc9

- No conclusions on a group level can be drawn now neither for the able-bodied individuals, nor for the stroke survivors. In the future, the VBMEG method can be applied on larger dataset.

6 Conclusion

This study evaluated the performance of the VBMEG method in brain source localization and dynamic information flow estimation. High Variance Accounted For was achieved by the VBMEG method on both able-bodied and stroke participants. Visualization of brain dynamic information flow intuitively shows the difference of brain function post stroke. Outcome of this study proves the feasibility of performing the VBMEG method on larger dataset to analyze the brain function changes post stroke statically. Application of the VBMEG method in stroke gives the chance of further understanding of neuroplasticity and has potential to help optimizing stroke treatments. Lateralization index and activation complexity was used, the first time, in detecting the brain function changes post stroke quantitatively with EEG measurements. This methodology fills the gap that conventional clinical tests cannot take insight brain function changes post stroke.

Bibliography

- AHN, D.-H., LEE, Y.-J., JEONG, J.-H., KIM, Y.-R. & PARK, J.-B. 2015. The effect of post-stroke depression on rehabilitation outcome and the impact of caregiver type as a factor of post-stroke depression. *Annals of rehabilitation medicine*, 39, 74-80.
- ARIKAN, K. 2011. Multimodal Brain Imaging. *Clinical EEG and neuroscience*, 42, x.
- ARYA, K. N., PANDIAN, S., VERMA, R. & GARG, R. 2011. Movement therapy induced neural reorganization and motor recovery in stroke: a review. *Journal of bodywork and movement therapies*, 15, 528-537.
- BACCALÁ, L. A. & SAMESHIMA, K. 2001. Partial directed coherence: a new concept in neural structure determination. *Biological Cybernetics*, 84, 463-474.
- BAILLET, S. & GARNERO, L. 1997. A Bayesian approach to introducing anatomo-functional priors in the EEG/MEG inverse problem. *IEEE transactions on Biomedical Engineering*, 44, 374-385.
- BAJAJ, S., BUTLER, A. J., DRAKE, D. & DHAMALA, M. 2015. Brain effective connectivity during motor-imagery and execution following stroke and rehabilitation. *NeuroImage: Clinical*, 8, 572-582.
- BANDARA, D., ARATA, J. & KIGICHI, K. Task based motion intention prediction with EEG signals. Robotics and Intelligent Sensors (IRIS), 2016 IEEE International Symposium on, 2016. IEEE, 57-60.
- BEAR, M. F., CONNORS, B. W. & PARADISO, M. A. 2007. *Neuroscience*, Lippincott Williams & Wilkins.
- BLINOWSKA, K. J., KUS, R. & KAMINSKI, M. 2004. Granger causality and information flow in multivariate processes. *Phys Rev E Stat Nonlin Soft Matter Phys*, 70, 050902.
- BREAKSPEAR, M. 2004. "Dynamic" connectivity in neural systems. *Neuroinformatics*, 2, 205-224.
- BRESSLER, S. L. & SETH, A. K. 2011. Wiener-Granger causality: a well established methodology. *Neuroimage*, 58, 323-9.
- BUCHNER, H., ADAMS, L., MÜLLER, A., LUDWIG, I., KNEPPER, A., THRON, A., NIEMANN, K. & SCHERG, M. 1995. Somatotopy of human hand somatosensory cortex revealed by dipole source analysis of early somatosensory evoked potentials and 3D-NMR tomography. *Electroencephalography and Clinical Neurophysiology/Evoked Potentials Section*, 96, 121-134.
- DALE, A. M. & SERENO, M. I. 1993. Improved localization of cortical activity by combining EEG and MEG with MRI cortical surface reconstruction: a linear approach. *Journal of cognitive neuroscience*, 5, 162-176.
- DELORME, A. & MAKEIG, S. 2004. EEGLAB: an open source toolbox for analysis of single-trial EEG dynamics including independent component analysis. *Journal of neuroscience methods*, 134, 9-21.
- DESMEDT, J. E. & CHERON, G. 1980. Somatosensory evoked potentials to finger stimulation in healthy octogenarians and in young adults: Wave forms, scalp topography and transit times of parietal and frontal components. *Electroencephalography and Clinical Neurophysiology*, 50, 404-425.
- DI CARLO, A. 2009. Human and economic burden of stroke. Oxford University Press.
- DRUSCHKY, K., KALTENHÄUSER, M., HUMMEL, C., DRUSCHKY, A., HUK, W., NEUNDÖRFER, B. & STEFAN, H. 2003. Somatosensory evoked magnetic fields following passive movement compared with tactile stimulation of the index finger. *Experimental Brain Research*, 148, 186-195.
- FINGELKURTS, A. A., FINGELKURTS, A. A. & KÄHKÖNEN, S. 2005. Functional connectivity in the brain—is it an elusive concept? *Neuroscience & Biobehavioral Reviews*, 28, 827-836.
- FRISTON, K. J. 2011a. Functional and effective connectivity: a review. *Brain connectivity*, 1, 13-36.
- FRISTON, K. J. 2011b. Functional and effective connectivity: a review. *Brain connectivity*, 1, 13-36.
- FUKUSHIMA, M., YAMASHITA, O., KNÖSCHE, T. R. & SATO, M.-A. 2015. MEG source reconstruction based on

- identification of directed source interactions on whole-brain anatomical networks. *NeuroImage*, 105, 408-427.
- GLADSTONE, D. J., DANELLS, C. J. & BLACK, S. E. 2002. The Fugl-Meyer assessment of motor recovery after stroke: a critical review of its measurement properties. *Neurorehabilitation and neural repair*, 16, 232-240.
- GRECH, R., CASSAR, T., MUSCAT, J., CAMILLERI, K. P., FABRI, S. G., ZERVAKIS, M., XANTHOPOULOS, P., SAKKALIS, V. & VANRUMSTE, B. 2008. Review on solving the inverse problem in EEG source analysis. *Journal of neuroengineering and rehabilitation*, 5, 25.
- GREFKES, C. & FINK, G. R. 2011. Reorganization of cerebral networks after stroke: new insights from neuroimaging with connectivity approaches. *Brain*, 134, 1264-1276.
- GREICIUS, M. D., KRASNOW, B., REISS, A. L. & MENON, V. 2003. Functional connectivity in the resting brain: A network analysis of the default mode hypothesis. *Proceedings of the National Academy of Sciences of the United States of America*, 100, 253-258.
- JAMALI, S. & ROSS, B. 2013. Somatotopic finger mapping using MEG: toward an optimal stimulation paradigm. *Clinical Neurophysiology*, 124, 1659-1670.
- JENKINSON, M., BECKMANN, C. F., BEHRENS, T. E., WOOLRICH, M. W. & SMITH, S. M. 2012. Fsl. *NeuroImage*, 62, 782-790.
- KALOGIANNI, K., DAFFERTSHOFER, A., VAN DER HELM, F. C., SCHOUTEN, A. C. & DE MUNCK, J. C. 2018a. Disentangling Somatosensory Evoked Potentials of the Fingers: Limitations and Clinical Potential. *Brain Topography*, 31, 498-512
- KALOGIANNI, K., DE MUNCK, J. C., NOLTE, G., VARDY, A. N., VAN DER HELM, F. C. & DAFFERTSHOFER, A. 2018b. Spatial resolution for EEG source reconstruction—A simulation study on SEPs. *Journal of neuroscience methods*, 301, 9-17.
- KAMIŃSKI, M., DING, M., TRUCCOLO, W. A. & BRESSLER, S. L. 2001. Evaluating causal relations in neural systems: Granger causality, directed transfer function and statistical assessment of significance. *Biological Cybernetics*, 85, 145-157.
- KWAKKEL, G., KOLLEN, B. & WAGENAAR, R. 2002. Long term effects of intensity of upper and lower limb training after stroke: a randomised trial. *Journal of Neurology, Neurosurgery & Psychiatry*, 72, 473-479.
- LANG, C. E., BLAND, M. D., BAILEY, R. R., SCHAEFER, S. Y. & BIRKENMEIER, R. L. 2013. Assessment of upper extremity impairment, function, and activity after stroke: foundations for clinical decision making. *Journal of Hand Therapy*, 26, 104-115.
- MAAIJWEE, N. A., RUTTEN-JACOBS, L. C., SCHAAPSMEERDERS, P., VAN DIJK, E. J. & DE LEEUW, F.-E. 2014. Ischaemic stroke in young adults: risk factors and long-term consequences. *Nature Reviews Neurology*, 10, 315.
- MOSHER, J. C., LEAHY, R. M. & LEWIS, P. S. 1999. EEG and MEG: forward solutions for inverse methods. *IEEE Transactions on Biomedical Engineering*, 46, 245-259.
- MURPHY, T. H. & CORBETT, D. 2009. Plasticity during stroke recovery: from synapse to behaviour. *Nature Reviews Neuroscience*, 10, 861.
- NELLES, G., SPIEKERMANN, G., JUEPTNER, M., LEONHARDT, G., MÜLLER, S., GERHARD, H. & DIENER, H. C. 1999. Reorganization of sensory and motor systems in hemiplegic stroke patients: a positron emission tomography study. *Stroke*, 30, 1510-1516.
- ONIZ, A., INANC, G., GUDUCU, C. & OZGOREN, M. 2016. Brain responsiveness to non-painful tactile stimuli prior and during sleep. *Sleep and Biological Rhythms*, 14, 87-96.

- PENNY, W. D., FRISTON, K. J., ASHBURNER, J. T., KIEBEL, S. J. & NICHOLS, T. E. 2011. *Statistical parametric mapping: the analysis of functional brain images*, Elsevier.
- PORCARO, C., COPPOLA, G., PIERELLI, F., SERI, S., DI LORENZO, G., TOMASEVIC, L., SALUSTRI, C. & TECCHIO, F. 2013. Multiple frequency functional connectivity in the hand somatosensory network: an EEG study. *Clinical Neurophysiology*, 124, 1216-1224.
- REUTER, M., SCHMANSKY, N. J., ROSAS, H. D. & FISCHL, B. 2012. Within-subject template estimation for unbiased longitudinal image analysis. *Neuroimage*, 61, 1402-1418.
- ROTHI, L. J. & HORNER, J. 1983. Restitution and substitution: Two theories of recovery with application to neurobehavioral treatment. *Journal of Clinical and Experimental Neuropsychology*, 5, 73-81.
- SAKKALIS, V. 2011. Review of advanced techniques for the estimation of brain connectivity measured with EEG/MEG. *Comput Biol Med*, 41, 1110-7.
- SATO, M.-A., YOSHIOKA, T., KAJIHARA, S., TOYAMA, K., GODA, N., DOYA, K. & KAWATO, M. 2004. Hierarchical Bayesian estimation for MEG inverse problem. *NeuroImage*, 23, 806-826.
- SCHULZ, R., BUCHHOLZ, A., FREY, B. M., BÖNSTRUP, M., CHENG, B., THOMALLA, G., HUMMEL, F. C. & GERLOFF, C. 2016. Enhanced effective connectivity between primary motor cortex and intraparietal sulcus in well-recovered stroke patients. *Stroke*, 47, 482-489.
- SCOTT, S. H. 2004. Optimal feedback control and the neural basis of volitional motor control. *Nature Reviews Neuroscience*, 5, 532.
- SMAJLOVIĆ, D. 2015. Strokes in young adults: epidemiology and prevention. *Vascular health and risk management*, 11, 157.
- SMIT, D. J., STAM, C. J., POSTHUMA, D., BOOMSMA, D. I. & DE GEUS, E. J. 2008. Heritability of "small-world" networks in the brain: a graph theoretical analysis of resting-state EEG functional connectivity. *Hum Brain Mapp*, 29, 1368-78.
- SRINIVASAN, R., WINTER, W. R., DING, J. & NUNEZ, P. L. 2007. EEG and MEG coherence: measures of functional connectivity at distinct spatial scales of neocortical dynamics. *J Neurosci Methods*, 166, 41-52.
- STRUJIS, J. N., VAN GENUGTEN, M. L., EVERS, S. M., AMENT, A. J., BAAN, C. A. & VAN DEN BOS, G. A. 2005. Modeling the future burden of stroke in The Netherlands: impact of aging, smoking, and hypertension. *Stroke*, 36, 1648-1655.
- TODOROV, E. & JORDAN, M. I. 2002. Optimal feedback control as a theory of motor coordination. *Nature neuroscience*, 5, 1226.
- VLAAR, M. P., SOLIS-ESCALANTE, T., VARDY, A. N., VAN DER HELM, F. C. & SCHOUTEN, A. C. 2017. Quantifying nonlinear contributions to cortical responses evoked by continuous wrist manipulation. *IEEE transactions on neural systems and rehabilitation engineering*, 25, 481-491.
- WANG, L., ZHANG, J., ZHANG, Y., YAN, R., LIU, H. & QIU, M. 2016. Conditional granger causality analysis of effective connectivity during motor imagery and motor execution in stroke patients. *BioMed research international*, 2016.
- WARD, N. S. 2017. Restoring brain function after stroke—bridging the gap between animals and humans. *Nature Reviews Neurology*, 13, 244.
- WEINSTEIN, M., GREEN, D., RUDISCH, J., ZIELINSKI, I. M., BENTHEM-MUÑIZ, M., JONGSMA, M. L., MCCLELLAND, V., STEENBERGEN, B., SHIRAN, S. & BASHAT, D. B. 2018. Understanding the relationship between brain and upper limb function in children with unilateral motor impairments: a multimodal approach. *European Journal of Paediatric Neurology*, 22, 143-154.
- WENDEL, K., VÄISÄNEN, O., MALMIVUO, J., GENCER, N. G., VANRUMSTE, B., DURKA, P., MAGJAREVIC, R.,

SUPEK, S., PASCU, M. L. & FONTENELLE, H. 2009. EEG/MEG source imaging: methods, challenges, and open issues. *Computational intelligence and neuroscience*, 2009, 13.